

Diode-Pumped and Packaged Acoustooptically Tunable Ti:Er:LiNbO₃ Waveguide Laser of Wide Tuning Range

K. Schäfer, I. Baumann, Wolfgang Sohler, *Associate Member, IEEE*,
H. Suche, *Associate Member, IEEE*, and S. Westenhöfer

(Invited Paper)

Abstract—Design, fabrication, and properties of an acoustooptically tunable Ti:Er:LiNbO₃ waveguide laser of up to 31-nm tuning range in the wavelength band $1530 \text{ nm} < \lambda < 1575 \text{ nm}$ are discussed. The laser cavity is formed by an Au mirror and a dielectric mirror as output coupler, both vacuum-deposited on the polished waveguide endfaces. As tunable intracavity wavelength filter with zero frequency shift, two monolithically integrated single-stage acoustooptical TE–TM-mode converters are used together with two polarization splitters operated as TE- and TM-pass polarizers, respectively. The minimum threshold of about 54 mW (coupled) pump power is obtained at $\lambda \approx 1561\text{-nm}$ emission wavelength for diode laser pumping at $\lambda_p \approx 1480 \text{ nm}$. With about 110-mW coupled pump power, up to 320- μW output power is achieved; the emission linewidth is 0.3 nm.

Index Terms—Acoustooptic filters, erbium doping, integrated optics, tunable amplifiers, tunable filters, tunable lasers, waveguide filters, waveguide lasers.

I. INTRODUCTION

DURING the last few years, a whole new class of optically pumped waveguide lasers of attractive properties has been developed in rare-earth-doped LiNbO₃ [1]–[3]. Among them, Er-doped devices lead to emission in the wavelength range $1530 \text{ nm} < \lambda < 1610 \text{ nm}$, which is of particular interest for fiber optical communications. Free-running CW lasers have been developed with six different frequencies [4], [5] and with optimized efficiency [6]. More advanced laser structures take advantage of the excellent electrooptical and acoustooptical properties of the LiNbO₃ substrate. With an intracavity electrooptic phase modulator, mode-locked lasers have been developed [7], [8]. With an intracavity acoustooptical wavelength filter, a tunable laser has been demonstrated [9]. However, the first tunable laser suffered from high intracavity losses preventing a wide tuning range and an acceptable output power and slope efficiency, respectively.

In this paper, we report an acoustooptically tunable laser of improved design with significantly increased tuning range

and output power. Such a laser is expected to have numerous potential applications in optical communications utilizing wavelength-division multiplexing (WDM) techniques. In Section II, the laser design and the principle of tunable laser operation are discussed. The fabrication and properties of the different laser components are the subject of Section III. In Section IV, pigtailling and packaging are described before the properties of the packaged laser are presented in Section V. Finally, Section VI gives some concluding remarks and an outlook.

II. LASER DESIGN AND PRINCIPLE OF OPERATION

The design of the tunable laser is schematically shown in Fig. 1. It has a symmetric (with respect to a horizontal axis) waveguide structure with two polarization splitters embedded nearly as a whole in a guiding channel for surface acoustic waves (SAW's). They can be excited via interdigital electrodes leading to effective acoustooptical polarization conversions of the guided optical modes in case of phase matching. Most of the waveguide structure is fabricated in an Er-diffusion-doped LiNbO₃ substrate. The laser has a Fabry–Perot cavity comprised of an Au mirror on the rear (left) waveguide end face and of a broad-band dielectric mirror as output coupler on the other side. The latter simultaneously serves as pump reflector to achieve double-pass pumping.

The key component of the laser is a monolithically integrated, active (Er-doped) wavelength filter utilized as a narrow-band acoustically tunable optical amplifier inside the waveguide cavity. It consists of the two polarization splitters and the enclosed amplifying acoustooptical polarization converter. Narrow-band wavelength filtering is achieved by a wavelength selective (phase-matched) acoustooptical mode conversion in combination with appropriate polarization filtering. As the acoustooptical interaction induces a frequency shift by the acoustical frequency (which would be doubled during a round trip inside the cavity), a second acoustooptical mode converter is needed to compensate this shift.

The laser can be operated with TM-polarized pump radiation leading to TE-polarized laser emission or vice versa. In the first mode of operation [see Fig. 1(a)], the pump light is guided to the bar states of the polarization splitters leading to optical amplification in the “upper” waveguides. The state

Manuscript received March 10, 1997. This work was supported in part by the European Community within the RACE-II Program under “EDIOLL” Project R2013. The work of K. Schäfer was supported by a fellowship from Deutsche Telekom AG.

The authors are with Angewandte Physik, Universität-GH Paderborn, D-33098 Paderborn, Germany.

Publisher Item Identifier S 0018-9197(97)07093-0.

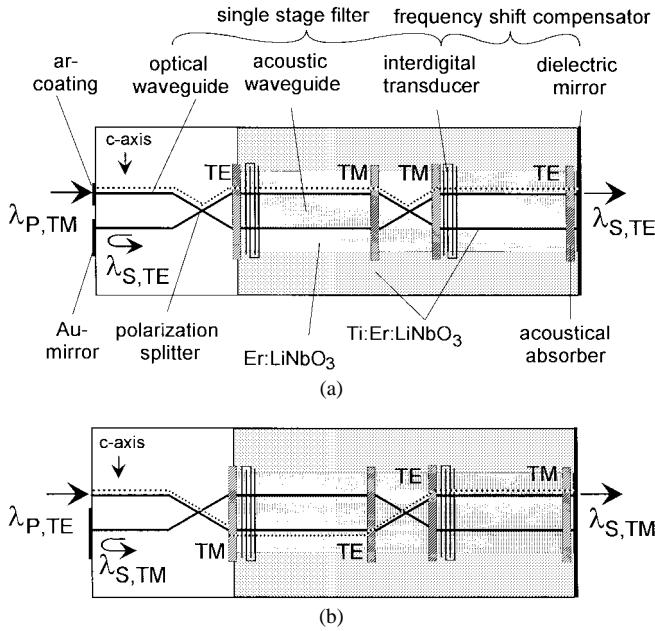


Fig. 1. Schematic diagram of the acoustooptically tunable Ti:Er:LiNbO₃ waveguide laser with a single-stage wavelength filter/frequency-shift compensator combination (a) for TM polarized pump leading to TE-polarized output and (b) for TE-polarized pump leading to TM-polarized output. The path of the pump (P) is given as dotted line. The states of polarization of the circulating resonant signal (S) are indicated by TE and TM within the mode converters.

of polarization of the pump is not influenced by both acoustooptical mode converters which define the laser emission wavelength. A phase-matched signal wave originating from spontaneous emission in the Er-doped waveguide sections can be resonantly amplified within the cavity, if it passes the wavelength filter/frequency-shift compensator combination in TE-polarization. A resonant wave undergoes four polarization conversions with accompanying frequency shifts during a round trip (from left to right in Fig. 1(a): TE, $f_0 \rightarrow$ TM, $f_0 + f_{ac} \rightarrow$ TE, $f_0 \rightarrow$ TM, $f_0 - f_{ac} \rightarrow$ TE, f_0 with $f_0 =$ laser emission frequency and $f_{ac} =$ SAW frequency). A mode of orthogonal polarization and of the same wavelength is directed in unpumped waveguide sections and absorbed. At others, unphase-matched wavelengths, a TM-polarized mode could lase if the upper left waveguide end face (the pump input) forms a cavity mirror of sufficient reflectivity; therefore, an antireflection coating is necessary.

In the second mode of operation [see Fig. 1(b)], the TE-polarized pump mode is guided to the cross states of the polarization splitters leading to optical amplification in the “lower middle” and “upper right” waveguide sections. In this case, a TM-polarized lasing mode is built up undergoing again four polarization conversions with corresponding frequency shifts during a round trip (from left to right in Fig. 1(b): TM, $f_0 \rightarrow$ TE, $f_0 - f_{ac} \rightarrow$ TM, $f_0 \rightarrow$ TE, $f_0 + f_{ac} \rightarrow$ TM, f_0).

III. LASER COMPONENTS

The essential laser components are described in more detail in the following. They comprise the Er-doped Ti:LiNbO₃ optical and acoustical waveguides (Section III-A), the integrated polarization splitters/pump coupler (Section III-B), the

amplifying acoustooptically tunable filter and frequency shift compensator (Section III-C), and the laser cavity (Section III-D).

A. Er-Doped Ti:LiNbO₃ Optical and Acoustical Waveguides

The fabrication of the Er-doped optical and acoustical waveguide structure has been performed in three steps: Er-diffusion-doping of the LiNbO₃ substrate, acoustical, and optical waveguide fabrication by Ti-indiffusion.

Due to the lower diffusion coefficients of Er compared to Ti, the surface doping of the X-cut LiNbO₃ substrate has been done first. A planar 22.1-nm-thick vacuum-deposited Er-layer, covering about three quarters of the surface, has been indiffused at 1130 °C during 135 h. These parameters lead to a nearly Gaussian concentration distribution of 6.2- μ m depth and a surface concentration of 1.3×10^{20} cm⁻³ [10].

As a second step, the 120- μ m-wide acoustical waveguide has been fabricated by defining its “claddings” via a deep indiffusion of 160-nm-thick evaporated Ti-strips at 1060 °C during 24 h. A nearly Gaussian concentration profile of 6.7- μ m depth and of 7.1×10^{20} cm⁻³ surface concentration results, yielding a monomode guide with undoped “core” for surface acoustic Rayleigh waves [11]. The propagation losses of the acoustical mode can be as low as <0.5 dB/cm.

Finally, the optical waveguide structure with the polarization splitters has been embedded symmetrically in the core of the acoustic guide: Photolithographically defined 7- μ m-wide Ti stripes of 98-nm thickness have been indiffused at 1060 °C during 8 h, resulting in a concentration distribution of 3.8- μ m depth and 1.2×10^{21} cm⁻³ maximum surface level. This distribution represents the core of monomode (at $\lambda \approx 1.55$ μ m) optical channel guides in the Er-doped substrate; only the left polarization splitter with short waveguide sections (see Fig. 1) has been fabricated in an undoped region.

For comparison, also straight channel guides without polarization splitters have been fabricated on the same sample in an Er-doped region. They allow an easier determination of scattering losses, absorption efficiency, and gain. Scattering losses of 0.1 dB/cm for TE-polarized light and 0.05 dB/cm for TM have been measured using the Fabry–Perot method [12] for the total loss and incoherent transmission measurements for the absorption part alone.

In Fig. 2, the transmittance through a straight doped waveguide is shown as a function of wavelength for different parameters of incident pump power from a pigtailed diode laser ($\lambda \approx 1480$ nm). Using fiber optic polarization controllers, pump and signal polarizations have been adjusted to σ (TM) and π (TE), respectively. This combination corresponds to the pump and emitted signal polarizations of the mode of operation of the tunable laser sketched in Fig. 1(a). Gain has been observed in the range from 1540 to 1580 nm with a maximum of 2 dB, indicating the possible tuning range of the laser to be developed.

B. Integrated Polarization Splitters/Pump Coupler

The splitters have been designed to guide TM-polarized light to the bar state and TE-polarized light to the cross state

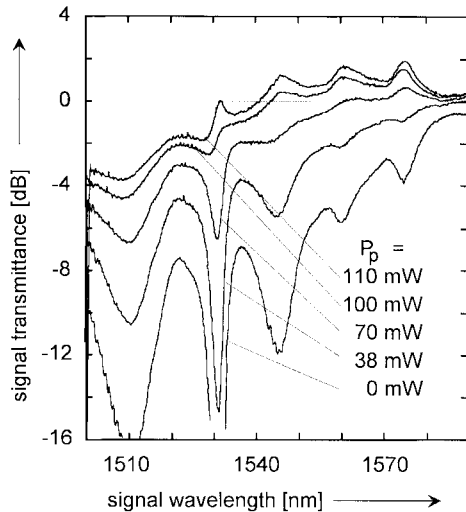


Fig. 2. Signal transmittance through a straight doped waveguide versus wavelength; parameter of the set of graphs is the incident pump power P_p ($\lambda_p \approx 1480$ nm). Pump (signal) polarization: TM (TE). The 0-dB line corresponds to the signal transmittance of a straight undoped waveguide.

[13]. They are zero-gap directional couplers with a two-mode, 14- μm -wide central section of 360- μm length and opening angles of 0.55° between the two single-mode waveguides on both sides. The measured splitting ratio of two devices cascaded in the laser structure is 13.9 dB for TE and 14.5 dB for TM. It might be erroneous to evaluate from these figures the data of a single polarization splitter alone; a possible slight asymmetry of the Mach-Zehnder-type structure would lead to phase differences between the waves passing the “lower” and the “upper” arms.

C. Amplifying Acoustooptically Tunable Filter and Frequency-Shift Compensator

Both acoustooptical polarization converters of the amplifying tunable filter and the frequency-shift compensator take advantage of the efficient acoustooptical interaction in the combined acoustical/optical waveguide structure (see Fig. 1). The optical guides are embedded in an acoustical one, yielding a good overlap of the interacting optical and acoustical waves and therefore low drive power levels to achieve full polarization conversion. The SAW in both converters is excited via separate interdigital transducers with 14 finger pairs and a periodicity $\Lambda = 20.8 \mu\text{m}$. The mode converters have interaction lengths of 13 mm (filter) and 11 mm (frequency shift compensator), respectively, defined by absorbing scotch tape strips across the acoustical channel guide.

The performance of the filter has been investigated first without optical pumping. A laser beam of 1557-nm wavelength has been coupled to the lower left input of the structure (see Fig. 1) to excite a TE mode. Then the filter characteristics was measured as the complementary notch response by monitoring the transmitted power of the lower right output as function of the acoustic frequency (see Fig. 3, left diagram). The SAW was excited in the filter only via the corresponding electrodes. With optimized RF-drive power of 15 dBm, a nearly full depletion is observed at the phase match frequency of 174.12 MHz,

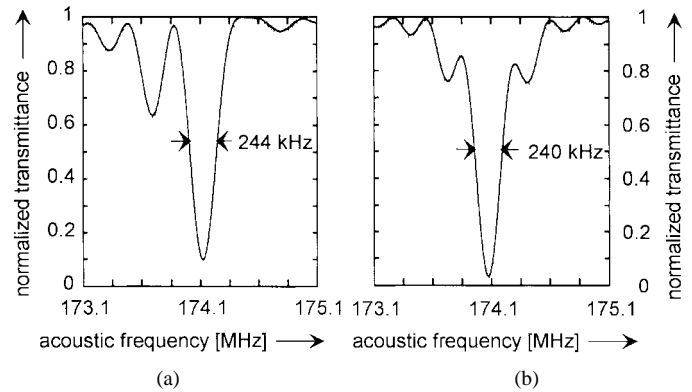


Fig. 3. Normalized transmittance at 1557-nm wavelength versus acoustic frequency for (a) the notch-filter and (b) the frequency shift compensator, measured without pumping of the filter structure. (The notch filter characteristic of the frequency-shift compensator was measured with an external polarizer.)

determined by

$$f_{ac} = \frac{v_{ac}}{\lambda} (n_{eff}^{TM} - n_{eff}^{TE}) \quad (1)$$

with

$$\begin{aligned} v_{ac}: & \text{acoustic phase velocity;} \\ \lambda: & \text{optical wavelength;} \\ n_{eff}^{TM,TE}: & \text{effective index of refraction of a TM- or TE-} \\ & \text{mode.} \end{aligned}$$

The residual transmission is due to a nonideal behavior of the polarization splitters. The pronounced sidelobe on the lower frequency side is caused by waveguide inhomogeneities. As mentioned, the filter characteristic is the complementary function; it could be measured at the upper right output also as transmittance versus wavelength at a fixed acoustic frequency. Both methods are nearly equivalent; wavelength and frequency scales are related via

$$\lambda(f_{ac}) \approx \lambda_m + \left. \frac{d\lambda}{df_{ac}} \right|_{f_m} (f_{ac} - f_m) \quad (2)$$

with

$$\begin{aligned} \lambda_m &= 1557 \text{ nm} \\ f_m &= 174.12 \text{ MHz} \\ \left. \frac{d\lambda}{df_{ac}} \right|_{f_m} &= -8.6 \text{ nm/MHz.} \end{aligned}$$

The halfwidth of 244 kHz of the notch response therefore corresponds to a halfwidth of 1.9 nm of the bandpass filter.

The performance of the frequency-shift compensator has been measured in the same way using the upper left input and TM polarization. The transmittance to the upper right output measured behind an external TM-pass polarizer characterizes the second polarization converter if the SAW is excited in the corresponding waveguide section only. The results are presented in the right diagram of Fig. 3. The measured transmission is closer to a theoretical response due to a better waveguide homogeneity.

Before depositing the laser mirrors, the whole structure has been investigated and optimized with optical pumping. TE-polarized radiation from an edge emitting, broad-band

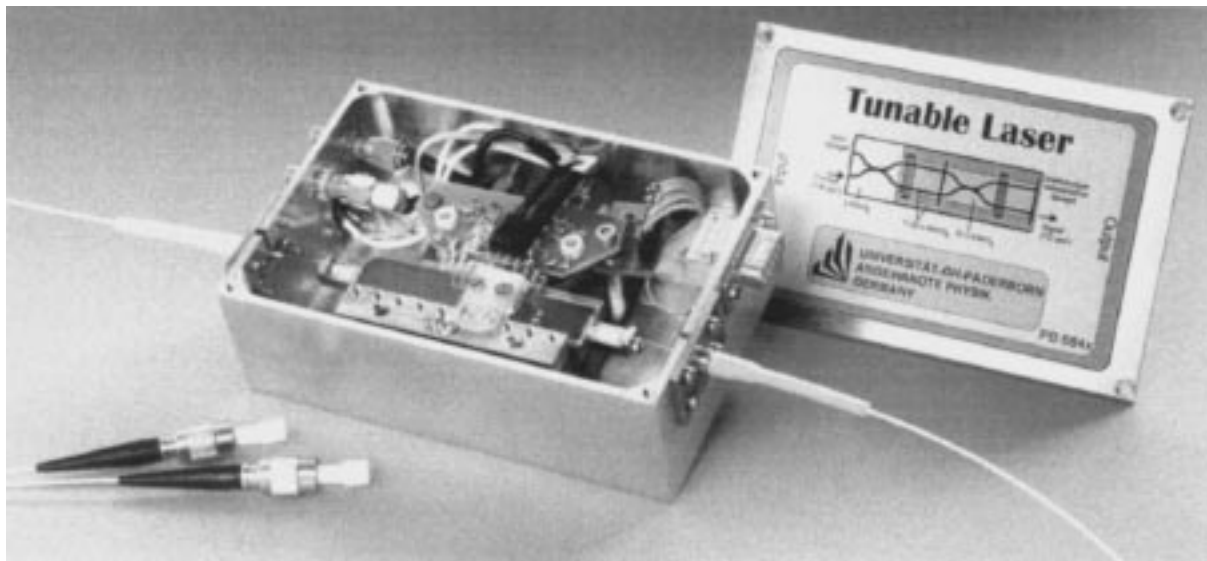


Fig. 4. Photograph of pigtailed and packaged acoustooptically tunable Ti:Er:LiNbO₃ waveguide laser.

luminescence diode ($1460 \text{ nm} < \lambda < 1620 \text{ nm}$) as signal and TM-polarized radiation from a laser diode ($\lambda \approx 1480 \text{ nm}$) as pump have been superimposed in a fiber optical WDM. They were launched into the upper right waveguide of the sample [see Fig. 1(a)] by butt coupling the common fiber output of the WDM. By differential temperature control and individual adjustment of the launched RF-power levels, the overall throughput of the Er-doped structure has been optimized. If both polarization converters are operated, the left polarization splitter separates pump and filtered (amplified) signal and facilitates in this way the measurement of the transmittance of both pump and signal radiation. Though the amplifying filter/frequency-shift compensator combination has additional losses in comparison to the straight doped waveguides on the sample ($\sim 0.2 \text{ dB}$ per transducer and $\sim 0.7 \text{ dB}$ per polarization splitter), similar gain spectra have been measured (see also Fig. 2). This is due to the twofold polarization conversion yielding a higher gain for TM–TM polarizations of pump and signal, respectively, than for the TM–TE combination.

D. Laser Cavity

The laser cavity consists of an Au mirror on the pump input side and a multilayer dielectric mirror on the signal output side. However, prior to the deposition of the mirrors, the pump input facet has been antireflection-coated for fiber coupling using a single vacuum-deposited Y₂O₃ layer, quarter-wave at about 1550 nm. Then the Au mirror has been selectively deposited on the end face of the lower branch of the left polarization splitter (see Fig. 1); it has a nearly wavelength-independent reflectivity in the range $1450 \text{ nm} < \lambda < 1600 \text{ nm}$ of about 95%. Finally, the signal output mirror has been vacuum-deposited on the right polished end face of the sample (see Fig. 1). It consists of 12 pairs of alternating layers of SiO₂ and TiO₂, respectively, quarter-wave at about 1500 nm. The high reflectivity of 98% at the pump wavelength of 1480 nm allows a double pass of the pump, thus improving the absorption efficiency. Within

the range of signal wavelengths $1530 \text{ nm} < \lambda < 1600 \text{ nm}$, the reflectivity changes only slightly from 98% to 97%.

IV. PIGTAILING AND PACKAGING

After characterization of the laser chip, single-mode (SM) fiber pigtailed with FC/PC-connectors at one end have been glued, using UV-curing epoxy, to the signal output facet and the AR-coated pump input facet, respectively. The fibers have been manually aligned during laser operation, using a fiber-pigtailed high-power laser diode (Alcatel A 1948 PLM) as pump source ($\lambda_p \approx 1480 \text{ nm}$). Subsequently, the pigtailed laser with submount for temperature control has been packaged in an Al housing with connectors for launching the RF drive signal to the interdigital transducers and for the temperature control. In Fig. 4, a photograph of the pigtailed and fully packaged acoustically tunable laser is shown. The cover of the housing has been removed to allow insight into the package. The laser chip on its temperature-controlled submount, the RF-impedance matching circuit of the transducers, and the attached fibers can be clearly seen.

V. CHARACTERIZATION OF THE PACKAGED DIODE-PUMPED LASER

The packaged Ti:Er:LiNbO₃ waveguide laser has been characterized in terms of power characteristics and tuning properties using a high-power diode laser as pump source. Moreover, with optically isolated output and feedback-controlled diode-pumping, the relative intensity noise (RIN) of the tunable laser has been determined.

The power characteristics of the tunable waveguide laser has been measured at the four different wavelengths 1531, 1546, 1561, and 1576 nm, adjusted by operating the acoustooptical polarization converters at 177.3, 175.4, 173.5, and 172 MHz, respectively. In Fig. 5, the results are plotted as the output power of the laser from the fiber pigtail versus the coupled pump power adjusted by the injection current of the pump laser diode. As its emission spectrum slightly shifts and broadens

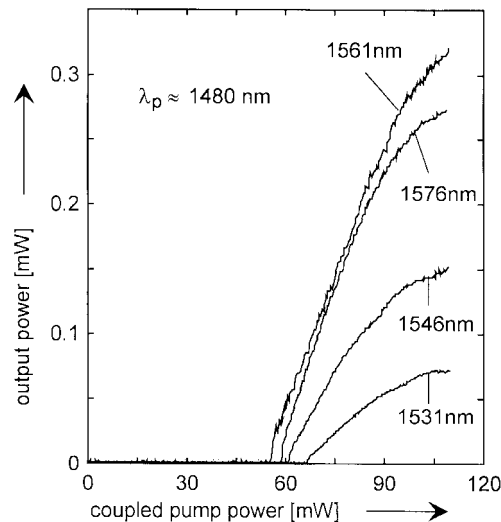


Fig. 5. Output power versus coupled pump power for diode-pumping of the pigtailed and packaged tunable Ti:Er:LiNbO₃ waveguide laser. Pump polarization: TM; signal polarization: TE.

with increasing drive current, the absorption efficiency of the Er-doped waveguide decreases correspondingly and a nonlinear power characteristics results. The slope efficiency is only about 0.7% at $\lambda = 1561$ and 1576 nm and even lower at the other emission wavelengths, indicating a great potential for further improvements by a reduction of the internal losses and by an optimization of the output coupling.

The tuning properties of the laser are shown in Fig. 6 together with a typical emission spectrum at 1562-nm center wavelength. The pump laser has been operated at the highest possible level yielding about 110-mW coupled pump power. Laser operation and tuning is achieved in four separate wavelength bands of a total width of 21.5 nm; they are found around the wavelengths of the maxima of the gain spectrum presented in Fig. 2 for 110 mW. The tuning bands broaden at higher pump power levels as demonstrated with a color center laser delivering about 180 mW; the total tuning range increases in this way to 31 nm. The tuning slope of -8.6 nm/MHz is determined by the phase match condition [see (1)] and therefore by the waveguide birefringence.

The linewidth of the laser emission of 0.3 nm is essentially determined by the bandwidth of the acoustooptical filter. The asymmetry of the spectrum shown in the inset of Fig. 6 is due to an imaging error of the monochromator.

To investigate the noise properties of the laser, the power density spectrum of the InGaAs photodetector current has been measured using an electronic spectrum analyzer. In Fig. 7, the results are shown as a function of frequency up to 100 MHz for a laser output power of 108 μ W, corresponding to a dc component of the detector current of 122 μ A or -31.3 -dBm electrical power dissipated in the 50- Ω input resistor of the spectrum analyzer. From both figures—RF-spectral power density and dc electrical power—the RIN of the tunable waveguide laser can be determined. For frequencies above 50 MHz, the RIN is below -125 dB/Hz. Due to the base level produced by the detector dark current, it cannot be assessed if the shot noise limit of -145.8 dB/Hz for the given laser

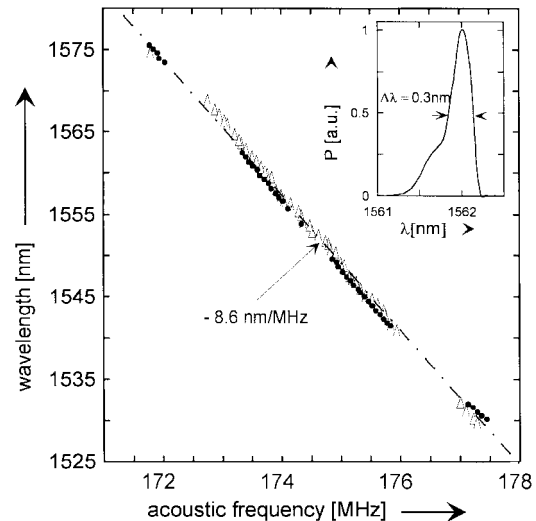


Fig. 6. Emission wavelength of the Ti:Er:LiNbO₃ waveguide laser versus acoustic frequency. Dots: diode-pumped ($P_p = 110$ mW) laser; triangles: color center laser pumped ($P_p = 180$ mW) laser. Dash-dotted line: straight line as guide of the eye. Pump polarization: TM. signal output polarization: TE. Inset: emission spectrum of the tunable laser at 1562-nm center wavelength.

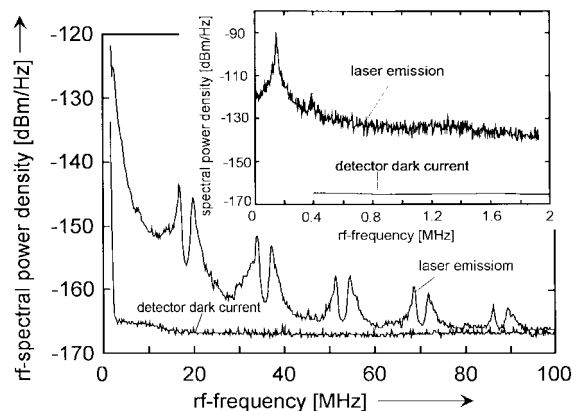


Fig. 7. RF-spectral power density of the detector current versus frequency for laser emission at 1561-nm wavelength. The dc electrical power corresponding to the average optical output power of the tunable laser of 108 μ W was -31.3 dBm. The spectra have been measured with a resolution bandwidth of 3 kHz at the lower frequencies (inset) and of 500 kHz at the higher frequencies.

output power is approached with increasing frequency. The double-peak structure of the laser noise spectrum around 18 MHz and higher harmonics is not yet understood. The range up to 2 MHz with the relaxation oscillation contribution to the noise spectrum is shown with higher resolution as inset. As a reference level, the noise spectrum of the detector dark current is given as well. This contribution almost coincides with the sensitivity limit of our spectrum analyzer. At the relaxation oscillation peak at about 150 kHz, the RIN increases up to -59 dB/Hz.

VI. CONCLUSION

We have reported the first pigtailed, packaged and diode-pumped acoustooptically tunable Ti:Er:LiNbO₃ waveguide laser. It has been significantly improved in terms of intracavity losses, threshold pump power levels, slope efficiency, and

especially output power compared to the properties of the tunable laser chip reported in [9]. Moreover, the laser RIN has been investigated. Future work will concentrate on the reduction of the intracavity losses and on the optimization of the laser cavity mirrors. In this way, continuous tuning from 1525 to 1580 nm wavelength is expected.

REFERENCES

- [1] E. Lallier, D. Papillon, J. P. Pocholle, M. Papuchon, M. De Micheli, and D. B. Ostrowsky, "Short pulse, high power q -switched Nd:MgO:LiNbO₃ waveguide laser," *Electron. Lett.*, vol. 29, no. 2, pp. 175–176, 1993.
 - [2] J. Amin, M. Hempstead, J. E. Roman, and J. S. Wilkinson, "Tunable coupled-cavity waveguide laser at room temperature in Nd-diffused Ti:LiNbO₃," *Opt. Lett.*, vol. 19, no. 19, pp. 1541–1543, 1994.
 - [3] I. Baumann, S. Bosso, R. Brinkmann, R. Corsini, M. Dinand, A. Greiner, K. Schäfer, J. Söchtig, W. Sohler, H. Suche, and R. Wessel, "Er-doped integrated optical devices in LiNbO₃," *J. Select. Topics Quantum Electron.*, vol. 2, pp. 355–366, 1996.
 - [4] R. Brinkmann, W. Sohler, and H. Suche, "Continuous-wave Erbium-diffused LiNbO₃ waveguide laser," *Electron. Lett.*, vol. 27, pp. 415–416, 1991.
 - [5] P. Becker, R. Brinkmann, M. Dinand, W. Sohler, and H. Suche, "Er-diffused Ti:LiNbO₃ waveguide laser of 1563 and 1576 nm emission wavelength," *Appl. Phys. Lett.*, vol. 61, pp. 1257–1259, 1992.
 - [6] I. Baumann, R. Brinkmann, M. Dinand, W. Sohler, and S. Westenhöfer, "Ti:Er:LiNbO₃ waveguide laser of optimized efficiency," *IEEE J. Quantum Electron.*, vol. 32, pp. 1695–1706, 1996.
 - [7] H. Suche, I. Baumann, D. Hiller, and W. Sohler, "Modelocked Er:Ti:LiNbO₃-waveguide laser," *Electron. Lett.*, vol. 29, pp. 1111–1112, 1993.
 - [8] H. Suche, R. Wessel, S. Westenhöfer, W. Sohler, S. Bosso, C. Carmanini, and R. Corsini, "Harmonically modelocked Ti:Er:LiNbO₃-waveguide laser," *Opt. Lett.*, vol. 20, pp. 596–598, 1995.
 - [9] I. Baumann, D. Johlen, W. Sohler, H. Suche, and F. Tian, "Acoustically tunable Ti:Er:LiNbO₃-waveguide laser," in *Proc. 20th Europ. Conf. Optical Communications, ECOC'94*, Florence, Italy, 1994, vol. 4, pp. 99–102.
 - [10] I. Baumann, R. Brinkmann, M. Dinand, W. Sohler, L. Beckers, Ch. Buchal, M. Fleuster, H. Holzbrecher, H. Paulus, K.-H. Müller, Th. Gog, G. Materlik, O. Witte, H. Stolz, and W. von der Osten, "Erbium incorporation in LiNbO₃ by diffusion-doping," *Appl. Phys. A*, vol. 64, pp. 33–44, 1997.
 - [11] H. Herrmann, U. Rust, and K. Schäfer, "Tapered acoustical directional couplers for integrated acousto-optical mode converters with weighted coupling," *J. Lightwave Technol.*, vol. 13, pp. 364–374, 1995.
 - [12] R. Regener and W. Sohler, "Loss in low-finesse LiNbO₃ optical waveguide resonators," *Appl. Phys. B*, vol. 36, p. 143, 1985.
 - [13] F. Tian, H. Herrmann, Ch. Harizi, V. Reimann, R. Ricken, U. Rust, W. Sohler, F. Wehrmann, and S. Westenhöfer, "Polarization independent integrated optical, acoustically tunable double stage wavelength filter in LiNbO₃," *Lightwave Technol.*, vol. 12, pp. 1192–1197, 1994.
- K. Schäfer**, photograph and biography not available at the time of publication.
- I. Baumann**, photograph and biography not available at the time of publication.
- Wolfgang Sohler** (A'88), photograph and biography not available at the time of publication.
- H. Suche** (A'95), photograph and biography not available at the time of publication.
- S. Westenhöfer**, photograph and biography not available at the time of publication.